TOTAL CROSS-SHORE SEDIMENT TRANSPORT UNDER SHOALING WAVES ON A STEEP BEACH

Troels Aagaard[1], Brian Greenwood[2] and Signe Mie Larsen[1]

Abstract

Acoustic backscatter measurements of suspended sediment transport in the lowest 50 cm of the water column were combined with bedform measurements to provide estimates of the total load sediment transport under shoaling waves on a steep, non-barred reflective beach. Large wave ripples were consistently present under conditions that exceeded commonly established thresholds for flat bed conditions. Net suspended sediment transport was approximately an order of magnitude larger than net bedload transport and the two transport components were oppositely directed under both storm-wave and low swell conditions.

Keywords: Bedforms, bedload, suspended load, PC-ADP, pencil-beam sonar.

1. Introduction

Since at least the mid-1970's there has been debate concerning the relative significance of bedload versus suspended load to the total and net transport of sediment under waves. This is an important issue since models of nearshore sediment transport usually separate transport into bedload and suspended load constituents and the hydrodynamic processes that mobilize and transport the sediment may be different for the two transport modes. The debate has been fuelled by measurement difficulties and hence difficulties with model validation. While suspended load can be measured relatively easily using optical or acoustic devices, direct quantification of bedload has proved considerably more difficult, especially under natural field conditions and very few field data sets exist that integrate observations of both modes of sediment transport.

While bedload is often impossible to quantify directly, it is generally recognized that it can be approximated indirectly by tracking bedform migration (e.g. Becker et al., 2007; van der Werf et al., 2007; Maier and Hay, 2009) and on that premise, Traykovski et al. (1999) used a combination of acoustic backscatter sensors and rotary side scan sonars to conclude that bedload was larger than suspended load by a factor of 20 in 11 m water depth off the east coast of the USA. On the other hand, Masselink et al. (2007) deployed sand ripple profilers and arrays of optical backscatter sensors in the intertidal zone of a coarse-grained beach in the UK and they found that suspended load was larger than bedload by a factor of 3-10. These examples illustrate that available field experimental evidence is highly contradictory on whether or not one or the other transport mode is more important. Based on these examples and similar evidence, it is likely that the balance depends on total bed shear stress such that suspended load becomes more dominant for large waves in shallow water.

[1]Institute of Geosciences, University of Copenhagen, Oster Voldgade 10, DK-1350 Copenhagen K., Denmark.
taa@geo.ku.dk
[2]Dept. of Physical and Environmental Sciences, University of Toronto Scarborough, Ontario M1C 1A4, Canada
greenw@utsc.utoronto.ca

Various types of bedload formulae have been proposed, mainly on the basis of laboratory experiments and some of them have been tested in the field. In the shallow nearshore (h < 3 m), Masselink et al. (2008) found that a Meyer-Peter and Müller (1948) type equation performed quite well, while the Bailard (1981) model underestimated the bedload transport that was estimated by tracking bedform geometry and migration speed. The bedload transport model of Ribberink (1998) which is based on the Meyer-Peter and Müller model was tested in a coarse-grained intertidal zone by Masselink et al. (2007) and it was found to underestimate bedload transport inferred from ripple migration. This was attributed to a suspended sediment transport contribution to bedform migration. On the other hand, Hay (2011) concluded that suspended sediment did not contribute to ripple migration since the Ribberink model worked quite well when bedforms were present in fine sand at 3-4 m water depth at Duck, US.

In this paper, we report field measurements of the total sediment transport under shoaling waves off a steep, reflective natural beach in 2.5-4 m water depth during high and low-moderate wave conditions. The shoreface sediment was composed of medium grained sand. Both suspended load and bedload transport were measured; the latter by using a pencil-beam sonar that recorded wave ripple dimensions and migration rate. The data were used to estimate the relative proportions of suspended and bedload transport and to test the Ribberink (1998) semi-empirical bedload formula for the migrating bedforms at the site. The measurements also provided information on ripple types and dimensions for different wave conditions; even though near-bed wave orbital velocities at times exceeded the flat bed-threshold for several hours, wave ripples were present consistently indicating considerable morphological hysteresis, or that the flat bed-threshold is inaccurate.

2. Field site and methods

A two-week field experiment was held at Pearl Beach on the northwest shore of the Broken Bay estuary, NSW, Australia during the period June 12-24, 2011. Pearl Beach is modally reflective and maintains this beach state virtually year round (Hughes and Cowell, 1987). The beach has a 960 m long zeta-shaped shoreline facing the incoming ocean swell with a modal deep-water significant wave height of 1.5 m and wave periods typically ranging from 8 to 14 seconds. The mean sediment grain size on the foreshore of Pearl Beach was 0.35-0.45 mm and the sand becomes finer on the lower shoreface, where the mean grain size was 0.25-0.30 mm at the instrument deployment positions.

During the field campaign, a storm occurred with 18-20 m s^{-1} wind speeds and offshore wave heights up to 4.5 m, although inshore wave heights were much lower due to wave refraction and diffraction into the estuary. A beach profile at the measurement site is shown in Figure 1. This profile was surveyed at the termination of the experiment and exhibited a slightly convex beach face with a wave-cut scarp that formed during the storm. Beach cusps with an average alongshore spacing of $\lambda \approx 30$ m persisted on the foreshore throughout the experimental period. Seaward of the step, another convexity was formed by sand eroded off the subaerial beach face during the storm and the instrument station used in this paper was located 25-30 m from the shoreline at the transition between this convexity and the concave lower shoreface (Figure 1).

The instruments that were used for hydrodynamic and sediment transport measurements were mounted on stainless steel tripods. Data in this paper derive from a station that was equipped with a Sontek 1.5 MHz Pulse-Coherent Acoustic Doppler Profiler (PC-ADP) programmed to record fluid velocity, pressure and acoustic backscatter at a rate of 2 Hz for periods of approximately 17 minutes (1024 s) each half-hour. Measurements of suspended sediment concentration and fluid velocity were obtained in the lowest 0.5 m of the water column with a vertical resolution of 1.6 cm. For bedform and bedload measurements, an Imagenex 881A pencil-beam sonar was used and fitted with an

azimuth drive for rotation of the sonar beam in the horizontal plane. The pencil-beam sonar was cantilevered off the tripod on a 1.5 m long stainless steel rod. Total sediment transport (bedload and suspended load) was measured during pre-storm, storm and post-storm conditions.

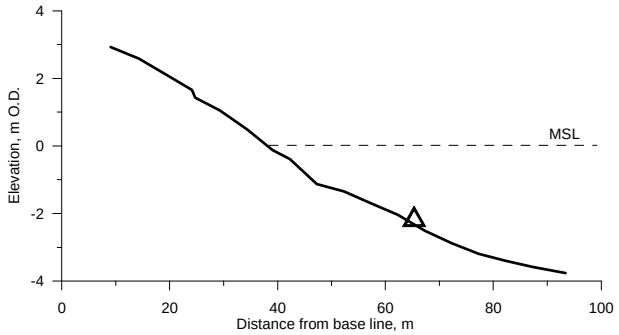

Figure 1. Cross-shore profile at the end of the experiment. The triangle marks the instrument tripod position.

Velocity outputs from the PC-ADP were rotated with respect to the orientation of the shore normal (66 degrees north) to provide cross-shore (u) and alongshore (v) velocities and these velocities were adjusted using the ambient speed of sound determined from a CTD-probe mounted on the instrument frame. With the selected settings, the horizontal velocity range of the instrument was 99 cm s^{-1}. When fluid velocities exceed the maximum velocity resolvable by the instrument, the velocity signal is wrapped resulting in erroneous readings. A second set of acoustic pulse pairs from the ADP allows the signal to be unwrapped, increasing the velocity range to 244 cm s^{-1} in the present configuration. Occasional data spikes in the velocity records were caused by low signal correlation and/or Doppler noise. Such spikes were replaced by a cubic spline interpolation and velocity data were subsequently smoothed using a fifth-order Butterworth low-pass filter with a filter cut-off of 0.67 Hz.

Time-dependent acoustic backscatter intensity was inverted to determine suspended sediment concentrations in the vertical using the approach described by Moate and Thorne (2012). In their notation, the acoustic sonar equation reads:

$$\ln(V_{rms} r \psi) = \ln(K_t K_s c^{½}) - 2r(\alpha_w + \alpha_s) \quad (1)$$

where V is acoustic backscatter intensity (measured in dB), c is sediment mass concentration, r is distance from the transducer head, ψ is a dimensionless near-field correction, K_t is a system constant, K_s is a constant that depends on sediment grain density, particle radius and the backscatter form function, α_w is sound attenuation due to water absorption, and α_s is sound attenuation due to sediment scattering. The system was calibrated in a recirculating water tank containing a known sediment mass concentration and regression of the term on the left-hand side of eq.(1) on r yields the second term on the right-hand side of the equation, this being the slope of the least-squares fit. This procedure allows determination of $K_t K_s$ and ultimately α_s, since α_w is a tabulated function. The equation is then inverted and solved sequentially from the uppermost measurement bin to the lowest bin using the implicit method (Thorne et al., 2011), which assumes that a_s is negligible over the 5 cm blanking distance at the top of the measured profile. Finally, since our interest lies with sand-sized sediment, backscatter offset was determined as the minimum output sound pressure for each measurement bin and subtracted from the signals. Predicted sediment concentrations (averaged over all three acoustic beams) were verified against independent measurements of sediment concentration from an optical backscatter (OBS) sensor. The ratio of C_{adp}/C_{obs} at the level of the OBS ranged from 0.60-1.47 with a mean of 0.89 which is considered good since the two instruments were not recording at the same

horizontal position relative to the rippled seabed.

The pencil-beam sonar was set at an initial elevation of 68 cm and depending on bedform height, good acoustic returns were obtained for cross-sections of the bed up to 250 cm long. At the beginning of each sonar recording session, the instrument orientation was set by rotating the sonar about the horizontal axis using the azimuth drive in order to maximize the bedform steepness in the bed return echo under the assumption that steepness is largest when the sonar beam is oriented perpendicular to bedform crests. Cross-sections of the bed were scanned continuously for periods of several hours. Sonar echoes that were more than 3 standard deviations from the mean bed position were removed first and the profiles were then smoothed using a 10-point window. High-concentration sediment plumes are a source of noise in pencil-beam data and noise was minimized by averaging bed elevation over 5 sonar scans, allowing the bed to be resolved at 3-minute intervals. Bedform height was computed as $\eta = 2\sqrt{2}\sigma_r$ (where σ_r is the standard deviation of the bed elevation) and the ripple migration speed C_r was determined from the lagged cross-correlation of bedform profiles, spaced 30 minutes apart to coincide with measurements of suspended sediment transport from the PC-ADP.

3. Results

3.1 Wave conditions

Measurements were made under shoaling waves seaward of the breakpoint and data from two separate 6-hour periods during the storm and post-storm phases are used in this paper. These two periods were selected because bedform migration was significant and consistently directed offshore and onshore, respectively. On both days, ripple crest orientation was within 5 degrees of the orientation of the shoreline. On the storm day (June 16), data were collected on a rising tide with increasing significant wave height, H_s = 0.65-0.98 m (Figure 2) and wave periods, $T_p \approx 12$ s at the instruments. Water depth (h) at the station increased from h = 2.5 to 4 m. On the post-storm day (June 19), data collection spanned low tide (h = 2-2.5 m) with H_s = 0.45-0.60 m and $T_p \approx 11$ s. On both days, depth-averaged Eulerian cross-shore current speeds varied between U = 0-0.07 m s^{-1} and longshore current speeds were V = 0-0.05 m s^{-1}.

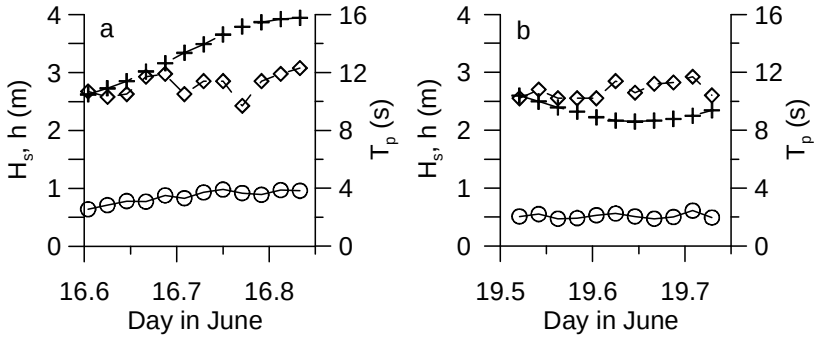

Figure 2. Inshore wave conditions for: (a) storm day (June 16) and (b) post-storm day (June 19). Circles denote the significant wave heights, diamonds are the peak spectral wave periods and crosses represent the mean water depths at the instrument position.

3.2 Ripple types and migration rates

At the beginning of each sampling sequence as noted earlier, the pencil-beam sonar was rotated through 180 degrees to determine ripple orientation and the sonar subsequently scanned a profile

oriented normal to bedform crests. Figure 3 illustrates bed profiles at the beginning and end of the data collection sequences on the two days. On both occasions, wave ripples were large. During the storm day (June 16), the ripples migrated offshore and ranged in height from η = 6.0-11.7 cm with an average of η = 8.0 cm. The ripple wavelength ranged between λ = 76-96 cm (mean λ = 85 cm and η/λ = 0.09). On the post-storm day (June 19), ripples migrated onshore, ranging in height from η = 6.5-12.0 cm (mean η = 9.7 cm) and λ = 57-77 cm (mean λ = 68 cm and η/λ = 0.14).

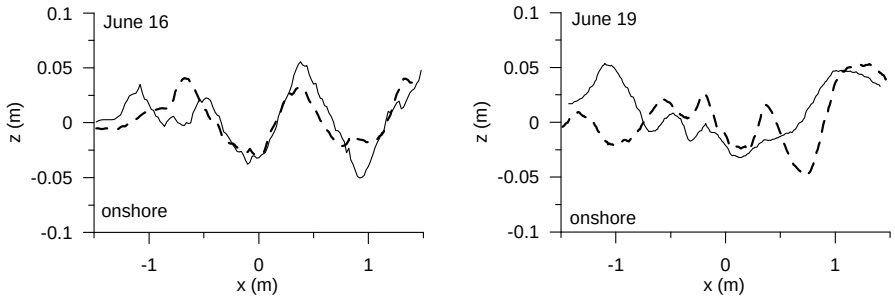

Figure 3. Bed profiles at the beginning (dashed) and end (solid lines) of the sonar sequences. *x* is the distance relative to the vertical sonar axis and *z* is the elevation relative to mean bed position.

Stacked bed profiles are illustrated in Figure 4. Wave ripples were present continuously during the 6-hour measurement sequences, but they migrated in opposite directions on the two days. On the storm day, the ripples migrated offshore with a mean speed of C_r = −12.2 cm h^{-1}. The persistence of the wave ripples on this day is rather unexpected, since mobility numbers were high (Figure 5). The mobility number is an implicit expression for the bed shear stress, and was introduced to avoid making assumptions about the friction factor; it is calculated as $\psi = u_s^2/((s-1)gD$, where u_s is the 'significant' horizontal orbital velocity, $(s-1)$ is relative sediment density, g is acceleration of gravity and D is mean sediment grain size. The threshold for flat bed conditions has been reported as ψ = 150-240 (Dingler and Inman, 1976; Gallagher et al., 2003; Hay and Mudge, 2005) and on the storm day, ψ = 160-361 such that the threshold was exceeded for periods of (at least) 1-2 hours. This may indicate significant bedform hysteresis. However, since ripple height initially increased rather than decreased as ψ exceeded the threshold (Figure 5), an alternative explanation might be that these thresholds are inaccurate for the coarse grain sizes at Pearl Beach.

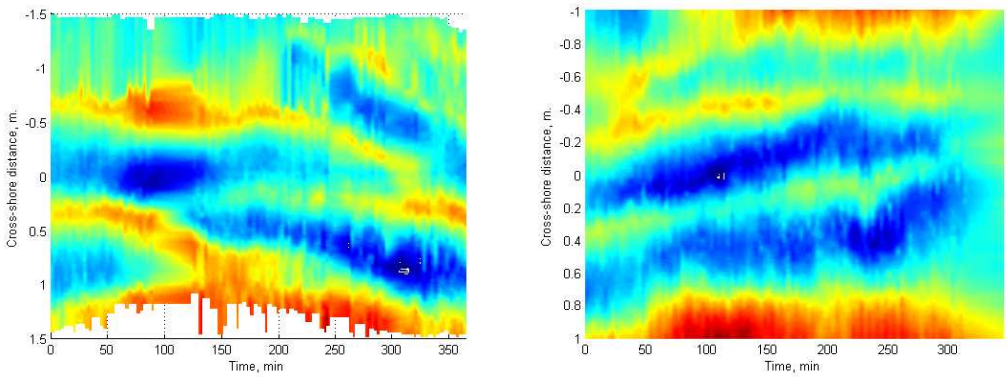

Figure 4. Time-distance diagrams of bed evolution and bedform migration on June 16 (storm day; left image) and June 19 (post-storm day; right image). N.B. Onshore is at the top of the images. Warm colours indicate positive deviations from mean bed elevation (i.e. ripple crests) and cold colours are negative deviations (ripple troughs).

On the post-storm day, ψ = 70-100 (Figure 5) and thus remained below the flat bed criterion. The wave ripples migrated onshore with a mean speed of C_r = +2.6 cm h^{-1} and migration rates were a factor 5 smaller than on the storm day.

Based on the work by Clifton and Dingler (1984), Wiberg and Harris (1994) distinguished between orbital-scaled ripples, which are stable when the ratio of wave orbital diameter to bedform height d_0/η < 12, suborbital ripples occur when 12< d_0/η< 100, and anorbital ripples exist when d_0/η >100. Further, O'Hara Murray et al. (2011) distinguished between vortex ripples which exhibit regular shedding of sediment-laden vortices from the bed, and post-vortex ripples where the shedding of vortices is less regular and coherent. The distinction was based on the ratio of λ/d_0 with vortex ripples occurring when the ratio is less than 0.83; Wiberg and Harris (1994) obtained a ratio of λ/d_0 = 0.65 for equilibrium vortex ripples. Based on these criteria, the bedforms can be classified as suborbital vortex ripples on the storm day. Frequent observations in the sonar images of suspended sediment clouds being lifted upward from the bed and dispersing during passage of large waves clearly showed the process of vortex shedding.

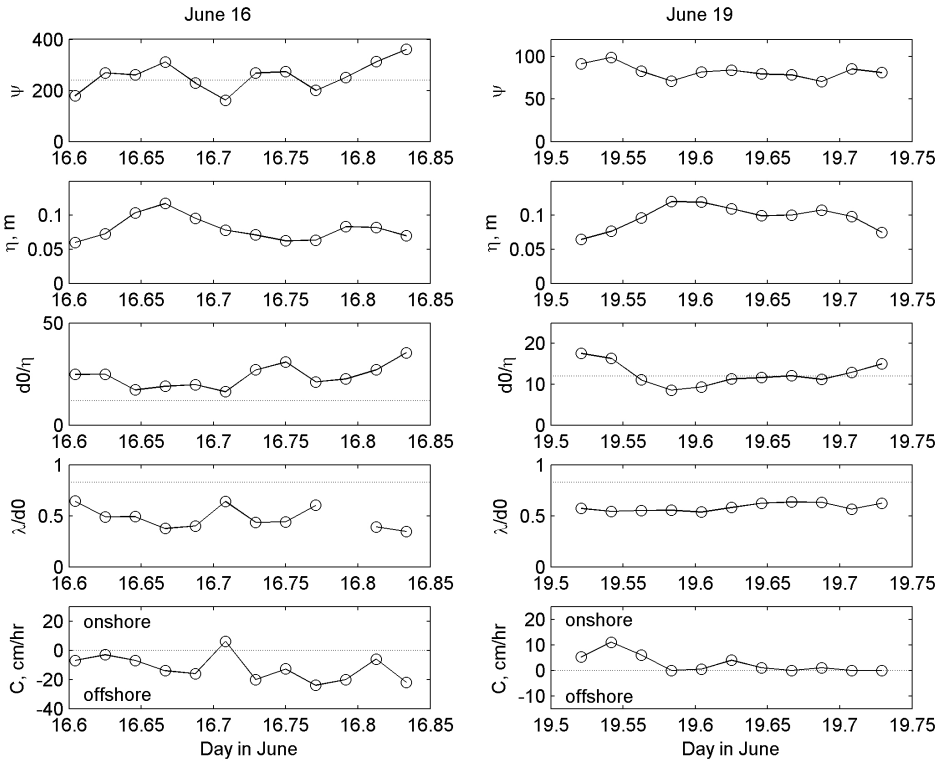

Figure 5. Bed state indicators on the two measurement days (June 16, storm day; June 19, post-storm day). From top to bottom, the panels show: Mobility number, ψ (the dashed line indicates the maximum flat bed threshold according to Dingler and Inman, 1976), ripple height, η, the ratio of orbital diameter to ripple height, d_0/η (the dashed lines signify the threshold for suborbital ripples according to Wiberg and Harris, 1994), the ratio of ripple wavelength to orbital diameter, d_0/λ (dashed lines indicate the upper threshold for vortex ripples, O'Hara Murray et al., 2011) and finally ripple migration speed, *C* where positive values indicate onshore migration.

On June 19, d_0/η fluctuated around a value of d_0/η = 12, and since λ/d_0 was close to 0.65 (Figure 5), the bedforms were classified as orbital-scaled vortex ripples.

3.3 Bedload and suspended load transport

Since the longshore transport of sediment in suspension accounted for less than 20% of the cross-shore transport, and since wave ripples migrated near to the shore-normal, we consider here only the cross-shore component of the sediment transport.

The net suspended sediment transport rate (per unit width of the beach), Q_s, was calculated from the PC-ADP measurements (Aagaard et al., 2012). For the storm day period, $Q_s = +4.0 \times 10^{-3}$ kg m^{-1} s^{-1} on average and it was directed onshore; for the post-storm day, average $Q_s = -8.9 \times 10^{-3}$ kg m^{-1} s^{-1} and was directed offshore (Figure 6). For both days combined, the mean transport component accounted for 80% of the total suspended transport while the oscillatory (intra-wave) component accounted for the remaining 20%. The onshore transport on the storm day was mainly caused by near-bed streaming since the Eulerian undertow was directed offshore (Aagaard et al., 2012). On the post-storm day, streaming was much reduced and the net offshore suspended transport was caused by both undertow and oscillatory wave motions.

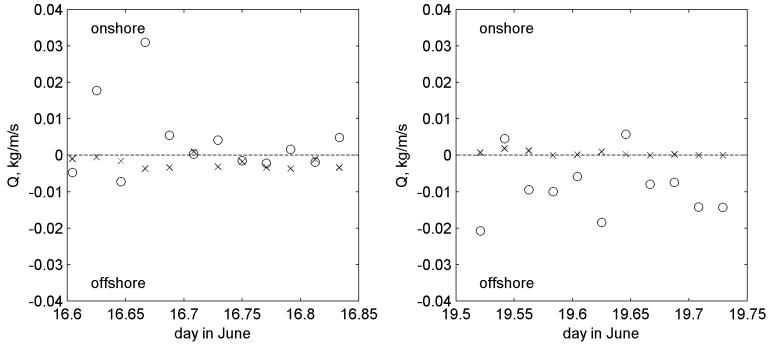

Figure 6. Bedload (crosses) and suspended load (circles) transport rates on June 16 (storm day) and June 19 (post-storm day).

Cross-shore mass transport through bedform migration was estimated as:

$$Q_r = \tfrac{1}{2}(1-a')\rho_s \eta C_r \cos\alpha \qquad (2)$$

where a' is the relative pore space volume, ρ_s is the sand density and α is the angle between ripple orientation and the shore-normal. The mean net bedload transport rate (Figure 6) for the storm day was $Q_r = -2.1 \times 10^{-3}$ kg m^{-1} s^{-1} (directed offshore) while for the post-storm day it was directed onshore, $Q_r = +4.9 \times 10^{-4}$ kg m^{-1} s^{-1}.

Bedload sediment transport models often correlate transport with fluid velocity skewness (Meyer-Peter and Müller, 1948; Bailard, 1981). In Figure 7, the bedload transport rate as inferred from bedform migration is plotted against the time-averaged total velocity skewness, $\langle u(t)^3 \rangle$. To ensure that velocities were obtained within the wave boundary layer, time series were extracted from three acoustic bins located between z = 2.5-5.5 cm above the ripple crests and skewness was calculated as the average over these bins. As shown in the figure, no trend was apparent between bedload transport

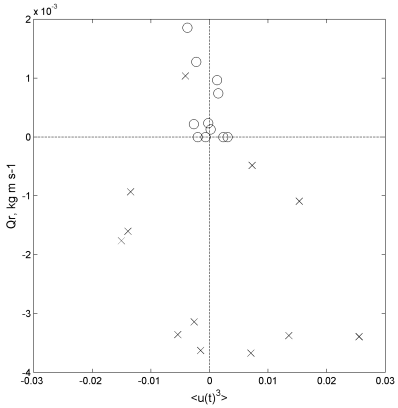

Figure 7. Bedload transport rate associated with ripple migration plotted against the time-averaged total velocity skewness in the wave boundary layer. Crosses: June 16, circles: June 19

and velocity skewness. The functional relationship did not improve when depth-averaged velocities or high-passed velocity skewness (to exclude mean currents and low-frequency waves) were used instead. In fact, wave height was a better predictor for bedload transport rate with a negative relationship existing between wave height and inferred transport rate.

The Ribberink (1998) semi-empirical bedload transport formula for combined wave-current flows relates transport to velocity (u) raised to the power of 3.3-3.5, instead of u^3. More elaborate quasi-steady bedload models exist such as TRANSKEW (Abreu et al., 2013) that take into account acceleration skewness. However, these models require a general waveform parameter that can be difficult to define for the natural irregular waves observed at Pearl Beach (Figure 8). The same velocity bins that were extracted above were used to evaluate the Ribberink model and as expected, model skill was low (Figure 9a). There is no apparent trend in the predictions, which are about an order of magnitude larger than measured transport rates. In fact, model predictions are more consistent with total (bedload plus suspended load) transport (Figure 9b). In this case, model trends can be identified, albeit being different for the two days (constants of proportionality $m \approx 5$ and 40, instead of $m = 11$; Ribberink, 1998), and measured and modeled transport rates are within the same order of magnitude with an $r^2 = 0.30$ and 0.52 for the two days.

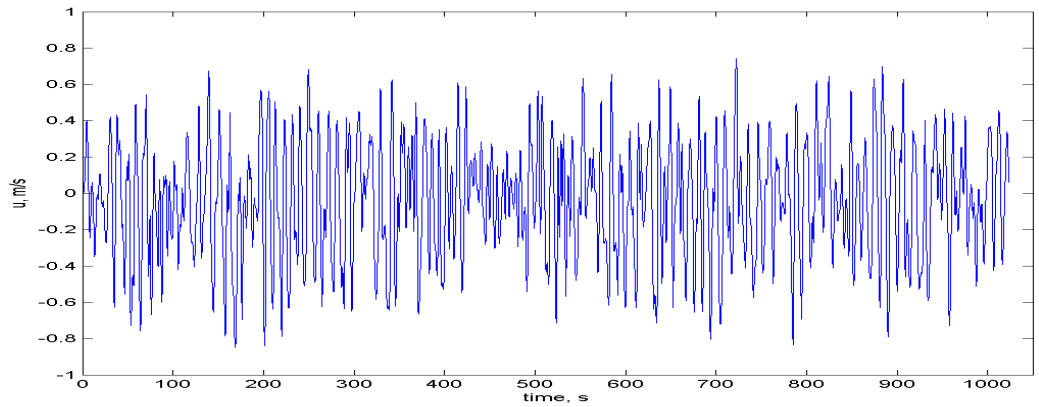

Figure 8. Cross-shore velocity time series on June 19 (post-storm day) at 1230 h. Positive velocities are onshore directed.

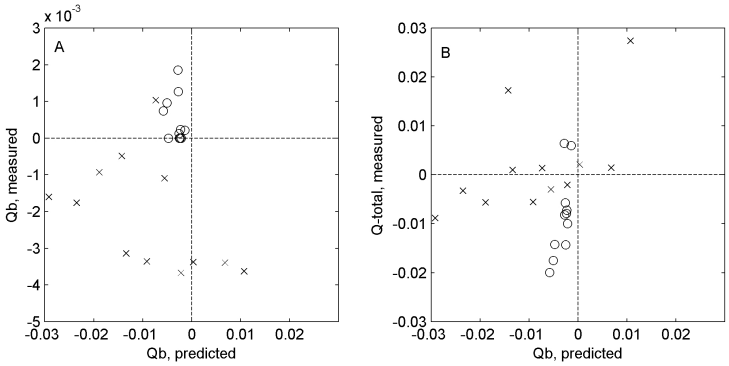

Figure 9. Measured bedload transport rate (A) and total load transport rate (B) plotted against predicted bedload transport rate from the Ribberink model. Crosses: June 16, circles: June 19.

4. Discussion

Under shoaling waves at Pearl Beach, wave ripples migrated offshore and onshore, respectively on two different days at speeds of 2.5-12 cm h^{-1}. These rates are of the same order as rates reported by Boyd et al. (1988) and Becker et al. (2007) in coarse-grained sand outside the surf zone. The bedforms at Pearl were classified as suborbital and orbital ripples, respectively on the two days; the ripples did not disappear, even though wave conditions resulted in large mobility numbers on the storm day. In fine grained sand (Mz = 0.15 mm) at Duck, N.C., the upper plane bed threshold has been reported as ψ = 150-200 (Gallagher et al., 2003; Hay and Mudge, 2005), but even though ψ > 300 for periods of more than one hour at Pearl, ripples were not planed off. In fact, ripple height increased as the mobility number increased on June 16 (Figure 5). This suggests a significant relaxation time, consistent with observations by Austin et al. (2007) and Hay (2011); alternatively, the flat bed threshold based on mobility number may not be universally applicable for different grain sizes and bedform dimensions.

Consistent with many earlier studies, bedload transport rates were assumed to be related to bedform migration. As expected, the largest bedload transport rates were measured on the storm day, when the average transport rate was approximately -2×10^{-3} kg m^{-1} s^{-1}; this is similar to estimates reported by Masselink et al. (2007) for shoaling wave conditions.

When comparing the inferred bedload ($Q_b = Q_r$) and measured net suspended load transport (Q_s) rates, two points are worthy of note: first, when averaged over individual 30-minute measurement periods, $Q_s/Q_b \approx 5$ for the storm day and $Q_s/Q_b \approx 22$ for the post-storm day (and for the entire 6-hour periods, $Q_s/Q_b \approx 2$ and 18, respectively for the storm and post-storm days). Hence, suspended sediment transport was significantly more important than bedload transport and the ratio between the two was again consistent with measurements reported by Masselink et al. (2007) in a study when suspended load was measured in the intertidal zone using optical sensors. However, while net bedload transport rates were larger on the storm day, as expected (Figure 6), net suspended sediment transport was not. The reason is that net Q_s involves several individual transport agents that often oppose one another: for example, undertow (offshore directed transport), near-bed boundary layer streaming and Stokes drift (onshore directed), and oscillatory transport (either direction). On the storm day, offshore transport due to undertow was significantly reduced, or even reversed by boundary layer streaming.

With the lower orbital velocities on the post-storm day, streaming was much reduced and this is consistent with numerical experiments of streaming over wave ripples (Vittori and Blondeaux, 2012). Hence, net Q_s was relatively small and onshore directed on the storm day while it was offshore directed and larger on the post-storm day.

Second, net bedload and net suspended load transports were opposed. On the storm day, the net suspended load was directed onshore and the net bedload was directed offshore. The opposite was the case for the post-storm observations. It is a commonly held notion (e.g. Aagaard and Masselink, 1999) that suspended load and bedload are typically transported in opposite directions with suspended load being driven offshore by undertow and bedload transport being driven onshore by orbital velocity skewness. While the former was overwhelmed by the effects of near-bed streaming on the storm day (Aagaard et al., 2012), the latter was clearly not the case here. Velocity skewness was small, whether expressed as total near-bed velocity skewness (and hence including mean currents in the wave boundary layer), or as a depth-averaged wave orbital skewness; skewness was often negative (offshore directed) and unrelated to the bedform migration rate (Figure 7). This indicates that either bedform migration rate cannot be equated with bedload transport, or bedload transport is not, at least for the large wave ripples found at Pearl, forced by velocity skewness above the ripple crests.

Unsurprisingly, tests of a commonly used bedload transport model (Ribberink, 1998) revealed no identifiable trends between this predictor and bedform migration. However, the fact that this limited data set exhibited reasonable correlation between the predictor and the total sediment transport (suspended load plus bedload) might suggest that the model is in fact a better predictor of total load rather than just bedload.

5. Conclusions

Field measurements of total sediment transport (bedload and suspended load in the lowest 50 cm of the water column) were conducted under shoaling waves on a medium-grained reflective beach. The following conclusions can be made from the experimental results:

a) suborbital ripples existed off Pearl Beach under conditions when established flat-bed thresholds were exceeded for several hours,
b) inferred net bedload transport rates were up to an order of magnitude smaller than the net suspended sediment transport rates,
c) although suspended load and bedload were transported in opposite directions, the present observations challenge commonly held beliefs on the major drivers of these transport modes.

Acknowledgements

We would like to express our gratitude to Dr. Alex Hay, Dalhousie University, for helpful advice on the sonar systems. Geoscience Australia constructed the instrument frames and Michael Hughes, Hannah Power and Paul Christiansen provided expert diving assistance.

References

Aagaard, T., Hughes, M., Baldock, T., Greenwood, B., Kroon, A. and Power, H., 2012. Sediment transport processes and morphodynamics on a reflective beach under storm and non-storm conditions. *Marine Geology*, 326-328, 154-165.

Aagaard, T. and Masselink, G., 1999. The Surf Zone. In: A.D.Short (ed) *Handbook of Beach and Shoreface Morphodynamics*. Wiley, Chichester, 72-118.

Abreu, T., Michallet, H., Silva, P.A., Sancho, F., van der A, D.A. and Ruessink, B.G., 2013. Bed shear stress

under skewed and asymmetric oscillatory flows. *Coastal Engineering*, 73, 1-10.
Austin, M.J., Masselink, G., O'Hare, T.J. and Russell, P.E., 2007. Relaxation time effects of wave ripples on tidal beaches. *Geophysical Research Letters*, 34, L16606
Bailard, J.A., 1981. An energetics total load sediment transport model for a plane sloping beach. *Journal of Geophysical Research*, 86, 10938-10954.
Becker, J.M., Firing, Y.L., Aucan, J., Holman, R., Merrifield, M. and Pawlak, G., 2007. Video-based observations of nearshore sand ripples and ripple migration. *Journal of Geophysical Research*, 112, C01007.
Boyd, R., Forbes, D.L. and Heffler, D.E., 1988. Time-sequence observations of wave-formed sand ripples on an ocean shoreface. *Sedimentology*, 35, 449-464.
Clifton, H. E. and Dingler, J.R., 1984. Wave-formed structures and paleoenvironmental reconstruction. *Marine Geology*, 60, 165-198.
Dingler, J.R. and Inman, D.L., 1976. Wave-formed ripples in nearshore sands. *Proc. 15th Int. Conf. Coastal Eng.*, Am.Soc. Civil Eng, New York, 2109-2126.
Gallagher, E.L., Thornton, E.B. and Stanton, T.P., 2003. Sand bed roughness in the nearshore. *Journal of Geophysical Research*, 108, 3039.
Hay, A.E., 2011. Geometric bed roughness and the bed state storm cycle. *Journal of Geophysical Research*, 116, C04017.
Hay, A.E. and Mudge, T., 2005. Principal bed states during SandyDuck97: occurrence, spectral anisotropy, and the bed state storm cycle. *Journal of Geophysical Research*, 110, C03013
Hughes, M.G. and Cowell, P., 1987. Adjustment of reflective beaches to waves. *Journal of Coastal Research*, 3, 153-168.
Maier, I and Hay, A.E., 2009. Occurrence and orientation of anorbital ripples in near-shore sands. *Journal of Geophysical Research*, 114, F04022.
Masselink, G., Austin, M.J., O'Hare, T.J. and Russell, P.E., 2007. Geometry and dynamics of wave ripples in the nearshore zone of a coarse sandy beach. *Journal of Geophysical Research*, 112, C10022.
Masselink, G.M., Austin, M.J., Russell, P.E. and O'Hare, T.J., 2008. Field investigations of wave ripple dynamics in the shallow nearshore of two sandy beaches. *Proceedings Int.Conf. Coastal Eng.2008*, ASCE.
Meyer-Peter, E. and Müller, R., 1948. Formulas for bedload transport. *Proc.Int.Ass. Hydr.Structures Res.*, Stockholm.
Moate, B.D. and Thorne, P.D., 2012. Interpreting acoustic backscatter from suspended sediments of different and mixed mineralogical composition. *Continental Shelf Research*, 46, 67-82.
O'Hara Murray, R.B., Thorne, P.D. and Hodgson, D.M., 2011. Intrawave observations of sediment entrainment processes above sand ripples under irregular waves. *Journal of Geophysical Research*, 116, C01001.
Ribberink, J.S., 1998. Bed-load transport for steady flows and unsteady oscillatory flows. *Coastal Engineering*, 34, 59-82.
Thorne, P.D., Hurther, D. and Moate, B.D., 2011. Acoustic inversions for measuring boundary layer suspended sediment processes. *Journal Acoustic Society of America*, 130, 1188-1200.
Traykovski, P., Hay, A.E., Irish, J.D. and Lynch, J.F., 1999. Geometry, migration and evolution of wave orbital ripples at LEO-15. *Journal of Geophysical Research*, 104, 1505-1524.
Van der Werf, J.J., Doucette, J.S., O'Donoghue, T. and Ribberink, J.S., 2007. Detailed measurements of velocities and suspended sand concentrations over full-scale ripples in regular oscillatory flow. *Journal of Geophysical Research*, 112, F02012.
Vottori, G. and Blondeaux, P., 2012. Sediment transport at the bottom of sea waves. *Proc.Int.Conf. Coastal Eng. 2012*, ASCE.
Wiberg, P.L. and Harris, C.K., 1994. Ripple geometry in wave-dominated environments. *Journal of Geophysical Research*, 99, 775-789.